UNDERSTANDING THE ROLE OF FORMIC ACID IN FINE AND COARSE PARTICLE MODE

A Thesis
Presented to
The Academic Faculty

By

Justin B. Min

In Partial Fulfillment
Of the Requirements for the Degree
Master of Science in the
School Earth and Atmospheric Sciences

Georgia Institute of Technology

August 2020

UNDERSTANDING THE ROLE OF FORMIC ACID IN FINE AND COARSE PARTICLE MODE

Dr. Rodney J. Weber, Advisor
School of Earth and Atmospheric Sciences
Georgia Institute of Technology

Dr. Nga Lee Ng
School of Chemical and Biomolecular Engineering
School of Earth and Atmospheric Sciences
Georgia Institute of Technology

Dr. Greg Huey
School of Earth and Atmospheric Sciences
Georgia Institute of Technology

Date approved: 20 July 2020

ACKNOWLEDGEMENTS

I would first like to thank Dr. Rodney Weber, my advisor, for challenging me to think critically about my research and for providing his expertise throughout my time at Georgia Tech. I am especially thankful for the opportunities he gave me to learn and become a better scientist. I would also like to extend my sincere thanks to my committee members, Drs. Sally Ng and Greg Huey, for their encouragement and taking the time to give me feedback on my thesis. Also thank you to Dr. Jenny Wong for helping me get adjusted into the research group and helping me think through my research projects. I am also grateful for other past mentors and advisors who kindled in me a strong interest in aerosol research, thank you to Drs. Roya Bahreini, Jim Smith, and Chongai Kuang for being a part of my journey.

I would like to thank past and present group members, Linghan, Yuhan, Dong, and Michael for sharing data with me and helping me find missing tools around the lab. A special thanks to Masayuki and Yunle for the formic acid data and being open for discussion which helped me better understand my research. Also thank you to Yoyin for teaching me how to use ISORROPIA when I did not have a clue. I am appreciative for the friends I made at Tech, thank you to Miguel, Melody, Louisa, Gabe, Raj, and Elise for filling me with laughter and being around for emotional support. A big thanks to my officemates, Derrick, Elizabeth, Tiegan, and Willi for your encouragement and support.

Lastly, I could not have made it this far without the support of my family and friends outside of Atlanta. Thank you to my mom and dad, for believing in me and loving me unconditionally. To Nara and Joe for taking the time to answer my calls and respond with

encouragement. To Gene and Becky for inviting me over during the holidays. Thank you to Vincent, Kimberley, and Danny for your friendship, love, and support.

TABLE OF CONTENTS

LIST OF TABLES

LIST OF FIGURES

LIST OF SYMBOLS AND ABBREVIATIONS

SYMBOLS

ε	Partitioning Coefficient
γ	Activity Coefficient
K_a	Dissociation Constant
$K_{x\text{-}FA}$	Stability Constant for Formic Acid

ABBREVIATIONS

aqSOA	Aqueous Phase Secondary Organic Aerosol
BrC	Brown Carbon
CIMS	Chemical Ionization Mass Spectrometer
JST	Jefferson Street
LWC	Liquid Water Content
LWCC	Liquid Waveguide Capillary Cell
NVC	Non-volatile Cation
OA	Organic Aerosol
MOUDI	Micro-Orifice Uniform Deposit Impactor
PILS-IC	Particle into Liquid Sampler coupled to Ion Chromatography
PM	Particulate Matter
PMF	Positive Matrix Factorization
SOA	Secondary Organic Aerosol
VOC	Volatile Organic Compound

SUMMARY

Formic acid partitioning was investigated at two sites in the southeast U.S., Yorkville, GA and Jefferson Street (JST). Previous studies in the southeast have shown that observed formic acid partitioning to fine particles did not agree with predicted partitioning due to very low predicted fine particle pH. This thesis looks to understand the possible causes for this discrepancy. The abundances of nonvolatile cations (NVCs) observed in particulate matter (PM) lead to the investigation of NVC complexation with formic acid to possibly provide additional insight on formic acid partitioning. Bulk particle pH and particle liquid water content were estimated using the ISORROPIA II thermodynamic model. Formic acid partitioning and pH results showed that assuming $PM_{1.0-2.5}$ was externally mixed from $PM_{1.0}$ at JST improved the agreement between the measured and predicted formic acid partitioning. This was only for $PM_{1.0-2.5}$ because the partitioning pH was closer to neutral. However, it could not resolve the disagreement with $PM_{1.0}$, suggesting that there may be different chemical processes and sources of formic acid that may be contributing to the fine and coarse mode. Increasing particle water concentrations also affected predicted partitioning of formic acid but were not sufficient to agree with observed partitioning. Correlations also indicate that formic acid in the southeast may be associated with mineral dust and biomass burning, suggesting a need to understand the source contributions of formic acid in more detail.

CHAPTER 1

INTRODUCTION

Aerosols are particles in a solid or liquid state that are suspended in the air. They have a variety of sizes and have different chemical compositions. Ambient aerosols can have a variety of sources, both primary (emitted directly) or secondary (formed in the atmosphere from emitted gases). These sources can be anthropogenic (e.g., vehicular emissions, industry, agriculture) and biogenic (e.g., vegetation, ocean wave breaking wind-blown dust) and are involved in different physical and chemical processes that affect human health, climate, and ecosystems. Typically, ambient aerosols are measured in bulk as $PM_{2.5}$ and $PM_{1.0}$, which are particles less than 2.5 μm or 1.0 μm aerodynamic diameter, respectively. $PM_{2.5}$ and $PM_{1.0}$ are important because they have long enough lifetimes in the atmosphere to undergo chemical transformations that can effect visibility, cloud processing, and health. These lifetimes can be in the order of days to weeks, during this time aerosols undergo additional processes to form secondary products and travel long distances (>1000 km) from their sources. Particles larger than 2.5 μm are seldom studied because they tend to have larger settling velocities that shorten their atmospheric residence times.

1.1 Motivation for studying inorganic aerosols

Atmospheric aerosols are complex mixtures composed of water, organics, inorganics (i.e., sulfate, nitrate, ammonium), elemental carbon, metals, and mineral dust. A large part of $PM_{2.5}$ (dry) mass (25-50%) is inorganic with ammonium, sulfate, nitrate, chloride, and sodium ions most commonly observed [Heintzenberg (1989)]; these species can have a significant impact on our ability to achieve $PM_{2.5}$ mass regulations to protect human health (e.g., EPA National Ambient Air Quality Standards, https://www.epa.gov/criteria-air-pollutants). Inorganic species

also significantly influence fine particle ($PM_{1.0}$) pH, which in turn, influences particle mass and composition by affecting the partitioning of semi-volatile organic and inorganics species between gas and particle phases [Guo et al. (2016)]. For example, gases such as NH_3 can partition into the particle phase, and since NH_3 emissions are connected to world food production, they are expected to increase as the world population grows [National Academies of Sciences et al. (2016)] thereby impacting $PM_{2.5}$ ammonium concentrations. In contrast, sulfate and nitrate concentrations are expected to decrease due to regulations on SO_2 and NO_x emissions [Stocker et al. (2013)]. These changes will likely have effects on particle pH, aerosol composition, and aqueous phase chemistry, with implications for health due to PM exposure [Pope III et al. (2004)], nutrient mobilization [Meskhidze et al. (2003)], and cloud formation [Gordon et al. (2017)].

1.2 Formic Acid Sources and Chemistry

This thesis focuses on studying particle phase formic acid (formate) because it is the simplest carboxylic acid and it is ubiquitous, in the troposphere. However, its sources and sinks are not well understood [Alwe et al. (2019)].Overall, total formic acid (gas + particle) concentrations are underestimated in models such as GEOS-Chem, suggesting that there is a large source of formic acid that is likely unaccounted. This is thought to be most likely secondary formation from oxidation of VOCs from biogenic sources, such as isoprene and terpenoids [Millet et al. (2015), Mungall et al. (2018), Veres et al. (2011), Xu et al. (2019)]. Other known sources include direct emissions from vehicle exhaust, biomass burning, biofuel burning, soil, and terrestrial vegetation [Paulot et al. (2011), Chaliyakunnel et al. (2016), Goode et al. (2000), Sanhueza et al. (1991)]. Formation of formic acid is also connected to anthropogenic precursors such as ethene, propane, and acetylene [Paulot et al. (2011)].

Typically, 98% of the total formic acid is measured in the gas phase [Millet et al. (2015)]. Similarly, studies in the southeast have shown formic acid is mainly in the gas versus fine particle phase [Nah et al. (2018), Liu et al. (2012)].

A major source of particle phase formic acid is from aqueous phase reaction of glyoxal with hydroxl radicals. The alkoxy radical produced from the reaction can decompose to yield formic acid [Lim et al. (2010)]. Additional studies have reported on formic acid in the particle phase [Sorooshian et al. (2007), Yu (2000), Liu et al. (2012), Nah et al. (2018)]. Due to its relatively low concentrations and widespread nature, the behavior of formic acid in the particle phase is not well understood. Some studies even attribute particle phase formic acid to positive artifacts from sampling processes [Yatavelli et al. (2014), Sorooshian et al. (2007), Williams et al. (2010)]. Equilibrium partitioning coefficients, a ratio of the particle phase to the total formic acid can help explain and interpret the behavior of formic acid in the particle phase. Partitioning is influenced by particle liquid water content, temperature, acid dissociation constants, pH, and activity coefficients. Formic acid has both a large Henry's law solubility constant (9540 mole L^{-1} atm^{-1} at 23.4°C) and large vapor pressure—4.6 kPa at 20°C. At constant temperature, a particle with high liquid water (>100 $\mu g/m^3$) content, such as a cloud or fog droplet, is likely to have formic acid in the particle due to Henry's law, the pH will be close to neutral, and the activity coefficient (γ) near 1 due to being in an extremely dilute state. When clouds or fogs are present and formic acid is mainly in the liquid drops, in these cases, formic acid can influence the acidity of clouds and fogs and affect acid wet deposition [Khare et al. (1999)]. Conversely, for particle conditions with relatively small liquid water content, as seen in $PM_{2.5}$, the lower pH, high activity coefficients (non-ideal solutions) would drive the formic acid to the gas phase. Nah et al. (2018) also showed that measured formic acid partitioning did not agree with predicted partitioning at low pH, that

is, the thermodynamic predictions were underestimating partitioning. Nah reported that the disagreement could not be explained by positive artifacts from carbon denuder not being 100% efficient at removing gases that are collected in the particle phase, incorrect Henrys law constants, or the presence of formic acid dimers in the aqueous phase that could have caused higher-than-predicted particle phase formic acid concentrations. The discrepancy between measured and predicted formic acid partitioning is a major topic of discussion in this thesis. A proposed hypothesis to explain this disagreement is the complexation of non-volatile cations (NVCs) with formate. Another reason for this disagreement may be due to the particles being externally mixed, rather than internally mixed, this will also be investigated.

1.3 Aerosol pH in the southeast

Particle pH is an important parameter because it can affect the physical and chemical properties of an aerosol. For instance, this can influence the rate of SO_2 oxidation and HNO_3 gas partitioning and particle volatility [Keene et al. (1998)]. Moreover, acidic particles (low pH) can lead to acid-catalyzed reactions that produce aqueous phase secondary organic aerosol (aqSOA), such as epoxide ring opening reactions [McNeill (2015)]. Also, organic acids can be oxidized by OH, NO_3, and O_3 through multiple pH dependent reaction pathways [Pye et al. (2019)]. Previous studies have shown that pH can also be size dependent, that is, aerodynamic particle diameters greater than 2.0 μm have a pH close to neutral, while submicron sizes less than 1.0 μm have pH's around 1 to 2 [Keene et al. (2004), Fang et al. (2017)]. Fine and coarse mode aerosol pH in general is difficult to measure quantitatively with traditional methods (eg. pH probe) because they have such small liquid volumes and sizes. Despite these limitations, thermodynamic equilibrium models have been used to estimate bulk aerosol pH. This study estimates aerosol pH

and aerosol liquid water content (LWC) using ISORROPIA II a thermodynamic model for inorganic aerosol systems.

CHAPTER 2

METHODS

2.1 Introduction

There are three locations where formate was measured, and they will be discussed in the following sections. The first location was in Yorkville, GA in 2016 and the second location was at Jefferson Street in Atlanta, GA in 2017, and the third location was at Georgia Tech in summer 2019. Yorkville and Atlanta are approximately 55 km apart and have different environmental factors. Yorkville is in a rural area while Atlanta is one of the largest metropolitan centers in the southeast US. The difference in anthropogenic and biogenic sources and spatial variability make data from these two areas unique. The data are used for further investigation of formic acid partitioning in the fine mode associated with varying sources and aerosol acidity.

2.2 Measurements at Jefferson Street

Daily ambient filter measurements were collected in 2017 at the Southeastern Research and Characterization (SEARCH) site in Atlanta, GA, which was located on Jefferson Street (JST) (33.777501°N, 84.416667°W), southwest of the Georgia Tech campus. Details of the site and methods can be found in Gao, et al. (2020). Particle sizes with aerodynamic diameters less than 2.5 μm ($PM_{2.5}$) were collected on Pallflex©Tissuquartz™ filters using a high-volume sampler at a flow rate of approximately 1.13 m^3/min. Filter samples were stored in a freezer until extraction and analysis. Cations and anions (ie. Ca^{2+}, Mg^{2+}, K^+, SO_4^{2-}, NO_3^-, Cl^-, and $CHOO^-$) were quantified by first extraction of circular filter punches sonicated in DI water for 30 min. Then filter extracts were analyzed isocratically using two Metrohm 761 Compact ICs, two separate columns, Metrosep C 4-150/4.0 and Metrosep A Supp 5-150/4.0 were used to measure cations

and anions, respectively. Total metal (all ion forms ie. Mg, Al, K, Ca, Cr, Mn, Fe, Cu, and Zn) concentrations were measured using inductively coupled plasma mass spectrometry (ICP-MS). Brown carbon was measured using a 1-m path length Liquid Waveguide Capillary Cell (LWCC-2100, World Precision Instrument, Sarasota, FL) with an internal volume of 250 µL. Dual deuterium and tungsten halogen light source (DT-Mini-2, Ocean Optics, Dunedin, FL) and absorption spectrometer (USB4000 spectrometer, Ocean Optics, Dunedin, FL) were coupled to the LWCC via fiber optic cables (QP400-2-SR, Ocean Optics, Dunedin, FL). Filter measurements have low time resolution because the concentrations are averaged over 24 hours. However, an entire year of filter measurements does provide seasonal variability of important ambient species.

2.3 Measurements in Yorkville, GA

Ambient measurements were made in another SEARCH site located in Yorkville, GA (33.928528ºN, 85.045483ºW), a rural site located 55 km northwest of Atlanta. Continuous ground-based measurements were conducted during the late summer and early fall season from August to October 2016. More detailed descriptions of the site are provided by Hansen et al. (2003). Gas phase measurements of ammonia, sulfur dioxide, nitric acid, and carboxylic acids, formic, oxalic, and acetic acid were made with a custom-built chemical ionization mass spectrometer (CIMS) using a hexafluoride (SF_6^-) ion source and a quadrupole mass spectrometer [Nah et al. (2018)]. Aerosol chemical composition was observed using two online particle into liquid sampler systems coupled to ion chromatographs (PILS-IC) sampling at 16.7 LPM. A URG $PM_{1.0}$ cyclone was used to collect particles with aerodynamic diameters less than 1.0 µm. Acidic and basic gases were removed via 2 URG glass annular denuders located upstream of the PILS-IC sampling line, one coated with sodium carbonate and the other with phosphorus acid. The

quantified water-soluble inorganics and organic acids were: SO_4^{2-}, NO_3^-, $C_2O_4^{2-}$, $CHOO^-$, CH_3COO^-, Cl^-, Na^+, Ca^{2+}, Mg^{2+}, and K^+. More detailed instrumentation and measurement techniques are elaborated in Nah et al. (2018).

2.4 MOUDI sampling at Georgia Tech

Size segregated particle filter samples were collected on the roof of the Georgia Tech Environmental Science and Technology building in Atlanta (33.779125ºN, 84.395797ºW). The roof is located approximately 30 to 40 m above ground level and about 800 m from the nearest traffic heavy interstate highway (I-75/I-85). A Micro-Orifice Uniform Deposit Impactor (MOUDI, MSP Corp., Shoreview, MN) with 11 stages was deployed from mid-May through early August of 2019. The MOUDI typically sampled during a one- week period at an average flowrate of 27.5 LPM at ambient temperature and relative humidity. Bulk (single filter) $PM_{2.5}$ samplers were deployed concurrently for mass closure comparison with MOUDI measurements. Ambient particles were all collected on 47 mm Teflon© filters (Zefluor™ 2.0 µm PTFE pore membrane filter) with the exception of a 37 mm bottom stage filter (Zefluor™ 2.0 µm PTFE pore membrane filter). The nominal cut-point of the particles collected with 50% collection efficiency were 18.0, 10.0, 5.6, 3.2, 1.8, 1.0, 0.56, 0.32, 0.18, 0.10, and 0.056 µm [Marple et al. (1991)]. At the end of collection periods the filter samples were placed in individual Petri dishes and stored in a freezer at -17ºC until filter extraction and analysis. Filters were usually analyzed within three days and extracted using 15 mL of 18 Mohm deionized water in pre-baked glass vials and sonicated for 30 min. The extracts were placed in polyvials with filter caps and loaded into an autosampler system (Dionex AS40). The sample volumes were separated into two halves and analyzed for cations and anions. The same Metrohm IC system detailed in section 2.2 was

used to measure particle formate, oxalate, ammonium, sulfate, calcium, potassium, sodium, and magnesium.

2.5 Particle pH Calculations

Bulk particle pH was determined using a thermodynamic equilibrium model ISORROPIA II [Fountoukis and Nenes (2007)]. ISORROPIA II takes inputs of multiple inorganic chemical species and calculates their equilibrium concentrations. The model was run in both reverse and forward mode to estimate the pH and LWC of the bulk aerosol. In reverse mode the inputs are temperature, relative humidity, and aerosol phase concentrations of NH_4^+ , SO_4^{2-} , Na^+, Mg^{2+}, Ca^{2+}, K^+, Cl^-, NO_3^- . In forward mode, the inputs include total (gas + particle) inorganic concentrations. ISORROPIA II assumes that all species input are internally mixed in the ambient aerosol and calculates the inorganic gas and particle phase concentrations of the input inorganic species from with phase partitioning can be determined. It also predicts the particle inorganic LWC and proton concentration, from which the bulk pH is determined. The model's strength is in the treatment of crustal species such as K^+, Ca^{2+}, Mg^{2+}, and Na^+, but one of the limitations is that it does not consider the participation of organics. However, the contribution of organics to pH are negligible in this study region [Guo et al. (2015)]. The bulk particle pH was calculated by

$$pH = -\log_{10} \gamma_{H+} H^+_{aq} \cong -\log_{10} \frac{1000 \gamma_{H+} H^+_{air}}{W_i}, \quad (1)$$

where γ_{H+} is the activity coefficient for hydronium ions (assumed equal to 1), H^+_{aq} is the proton concentration [mol/L] in particle liquid water, H_{air}^+ is the proton concentration in µg per cubic meter of air, 1000 is the density term for water [kg/m^3], W_i is the bulk liquid water content associated with inorganic species in $\mu g/m^3$ of air. H_{air}^+ and W_i are outputs from ISORROPIA II and so the bulk pH can be calculated using equation (1).

Forward mode was run for both bulk particle pH estimations in $PM_{2.5}$ and $PM_{1.0}$ at JST and Yorkville, respectively. At JST, the inputs of the mass concentrations of NH_3 and HCl gas were assumed to be the same as that in Fang et al. (2017).

Size resolved pH was also obtained from MOUDI stages which were also run in forward mode. However, ISOROPPIA II inputs must include gas phase NH_3, HCl, and HNO_3 and during the MOUDI sampling period, size resolved particle phase NO_3^- and Cl^- were not measured and gas phase data such as NH_3, HCl, and HNO_3 were unavailable. So particle NO_3^- and Cl^- and gas phase NH_3 ,HNO_3, and HCl were based on estimations from the same sampling location, but different observation periods (spring 2016 versus summer 2019) [Fang et al. (2017)], it was assumed that NO_3^-, Cl^-, HNO_3, NH_3 and HCl mass concentrations did not change significantly in between those years. Gas phase HNO_3 was also obtained from ambient measurements from a FIGAERO-HR-ToF-CIMS sampling at JST during August 2017, so the partitioning of formic acid with respect to pH at JST is focused only on the month of August. The average mass concentrations for gas phase HNO_3, NH_3, and HCl used in size resolved pH calculations were 0.674, 0.70, and 2.2 µg/m3, respectively. ISORROPIA II was run in forward mode with total gas and particle phase concentrations for cut-off sizes less than 1.8 µm. For cut-off sizes greater than 1.8 µm the gas phase concentrations were assumed to be zero while running in forward mode, this was due to kinetic limitations that can inhibit coarse mode particles from reaching equilibrium with gases. It has also been shown that assuming coarse mode particles in equilibrium with the gas phase will lead to a large positive bias between predicted particle phase NO_3^- and NH_4^+ [Fang et al. (2017)]. Predicting coarse mode pH that is not in thermodynamic equilibrium with a thermodynamic model will introduce a large source of uncertainty. In a

previous study Fang et al. (2017) showed that with this uncertainty the coarse mode pH would range from approximately 4 to 7, but likely remain in the neutral region.

2.6 Formic Acid Partitioning Calculations

The relationship between gas and particle phase concentrations of a chemical species are studied by looking at partitioning ratios, which is the concentration of a chemical in the particle phase over its total concentration (gas + particle). Analytical solutions to calculate the partitioning of organic acids, such as acetic acid and formic acid partitioning, have been done by Nah et al. (2018), based on Henry's law. This thesis adds to this by also considering formic acid partitioning via complexation with NVCs (nonvolatile cations, such as Ca^{2+}, Mg^{2+}, K^{+}, and Na^{+}), which is not considered in the thermodynamic model. The analytical solution for formic acid partitioning that includes complexation was derived from Henry's law (equation 2) and equilibrium reactions (equation 3-7), where Equation (3) expresses the dissociation of formic acid in an aqueous solution, including activity coefficients, and Equations 4 – 7 are the new equilibrium reactions added that include complexation of dissociated formic acid with NVCs:

$$H_{HCOOH} = \frac{\gamma_{HCOOH}[HCOOH]}{P_{HCOOH}}, \tag{2}$$

$$K_a = \frac{\gamma_{H^+}[H^+]\gamma_{HCOOH}[HCOO^-]}{\gamma_{HCOOH}P_{HCOOH}}, \tag{3}$$

$$K_{Ca-FA} = \frac{[CaCHOO^+]}{[Ca^{2+}][HCOO^-]}, \tag{4}$$

$$K_{Mg-FA} = \frac{[MgCHOO^+]}{[Mg^{2+}][HCOO^-]}, \tag{5}$$

$$K_{K-FA} = \frac{[KCHOO]}{[K^+][HCOO^-]}, \tag{6}$$

$$K_{Na-FA} = \frac{[NaCHOO]}{[Na^+][HCOO^-]}, \quad (7)$$

The stability constants for the calcium formate ($K_{Ca\text{-}FA}$), magnesium formate ($K_{Mg\text{-}FA}$), potassium formate $K_{K\text{-}FA}$, and sodium formate $K_{Na\text{-}FA}$ complex, is shown in Equations 4, 5, 6, and 7, respectively. Equations 8 & 9 were derived from equations 2-7:

$$[X]_{aerosol} = 10^{-9} \cdot W \cdot K_{HCOOH} \cdot H \cdot R \cdot T \cdot \left(\frac{\gamma_{H^+} \cdot \gamma_{HCOO^-} \cdot [H^+]}{K_{HCOOH} \cdot \gamma_{HCOOH}} + 1 + K_{K-FA} \cdot [K^+] + K_{Ca-FA} \cdot [Ca^{2+}] + K_{Mg-FA} \cdot [Mg^{2+}] + K_{Na-FA} \cdot [Na^+] \right), \quad (8)$$

$$[X_{gas}] = \gamma_{H^+} \cdot \gamma_{CHOO^-} \cdot [H^+], \quad (9)$$

$$\varepsilon(X) = \frac{[X]_{aerosol}}{[X]_{gas} + [X]_{aerosol}}. \quad (10)$$

Where Equation 8 is equal to the concentration of formic acid in the particle phase. W is the average liquid water content estimated to be 1.6 μg/m^3, K_{HCOOH} is the formic acid dissociation constant (1.78*10^{-4} M), H = 9540 M/atm is the Henry's law coefficient for formic acid, the gas constant R = 8.21*10−5 m^3*atm*mol^{-1}K^{-1}. The activity coefficient of H^+ (γ_{H^+}) was equal to 1, the activity coefficient of formate (γ_{HCOO^-}) and formic acid gas (γ_{HCOOH}) was equal to 0.07 and 0.334, respectively. These activity coefficients are from Nah et al. (2018). Stability constants for formic acid and NVCs with $K_{K\text{-}FA}$ = 0.45, $K_{Ca\text{-}FA}$ = 100.27, $K_{Mg\text{-}FA}$ = 100.34, and $K_{Na\text{-}FA}$ = 0.31 were obtained from literature (Bunting and Thong (1970), Hiller (1966)). Equation 9 give the gas phase concentration of formic acid. Equations (8 & 9) can be substituted into equation (10) the general partitioning equation where $[X]_{gas}$ denotes the concentration of species x in the gas phase and $[X]_{aerosol}$, the concentration of species x in the particle phase.

CHAPTER 3

RESULTS

Observations from Yorkville, GA and Atlanta, GA are highlighted in this section. Equivalence concentrations of formate and acetate were compared to NVCs, the correlations and slopes indicated that NVCs could complex with particle phase formic acid. The change in formic acid partitioning pH due to NVC complexation with formate is studied using the S-curves from the analytical solution. In addition, the discrepancies between formic acid predicted and observed partitioning were further probed by looking at sensitivity to temperature, liquid water content, and external mixing states.

3.1 Yorkville Correlations and Nonvolatile Cation Complexation

Formic acid in the particle phase has weak diurnal trends in Yorkville, while gas phase has clear diurnal trends according to Nah et al. (2018). In the gas phase, formic acid concentrations peak at around 18:00 EST and decrease and gradually increase around 7:00 EST. The gradual increase in formic acid gas could be due to the photooxidation of volatile organic compounds (VOCs) that might lead to the production of formic acid. Glyoxal oxidation in the aqueous phase could also be a source of formic acid [Lim et al. (2010)].

The average conditions during the Yorkville study were as follows. Average temperature was 24.0^{o}C with minimum and maximum temperatures observed at 9.5^{o}C and 32.6^{o}C, respectively. Relative humidity (RH) was the highest before sunrise, the average RH was 68.9% while the minimum and maximum RH was 21.6% and 100%, respectively. Detailed meteorological data is shown in [Nah et al. (2018)]. The average fine particle pH was calculated

by Nah et al. at 2.52 (± 1.3) and is similar to pH reported in previous studies conducted in the southeast [Guo et al. (2015)].

Table 1: Table of mean mass concentrations of relevant cations and anions measured in Atlanta, GA and Yorkville, GA. Atlanta, GA has higher mean cation concentrations most likely due to anthropogenic sources. Yorkville has higher anion concentrations of formate and acetate when compared to Atlanta, GA.

Anions & Cations	**Jefferson Street 2017 (µg/m^3)**	**Yorkville 2016 (µg/m^3)**
Ca^{2+}	0.120 ±0.12	0.020 ±0.009
Mg^{2+}	0.017 ±0.020	0.0020 ±0.001
K^{+}	0.048 ±0.038	0.035 ±0.011
Na^{+}	N/A	0.021 ±0.005
$CHOO^{-}$ (Formate)	0.026 ±0.018	0.050 ±0.023
CH_3COO^{-} (Acetate)	N/A	0.064 ±0.022
$C_2O_4^{2-}$ (Oxalate)	0.110 ±0.065	0.058 ±0.037

Average ambient mass concentrations of NVCs, formate, and acetate are shown in Table 1. All concentrations are low, in the 10s of ng/m^3, or less. JST and Yorkville are side by side in Table 1 for comparison. It should be noted that JST mass concentrations are a different cut off size, that is $PM_{2.5}$ compared to Yorkville which is $PM_{1.0}$. At Yorkville, good correlations (R) were observed between formate and NVCs ($R_{K+} = 0.59$, $R_{Ca2+} = 0.46$, and $R_{Mg2+} = 0.52$), these results are shown in Table (2). Sodium is left out of the correlation because few measurements were above the instrument LOD for the sampling period. For this reason, an average Na^+ concentration was estimated by using the relationship between Na^+ and Cl^-. One mole of sodium was assumed to be equal to one mole of chloride, then the moles of sodium was corrected by multiplying by a factor of 0.84, which was the average Na:Cl ratio from the limited measurements.

Table 2: Shown below are correlation coefficients [R] between different cations and anions from filter samples (JST) and online sampling (YRK). Different seasons at JST are shown to highlight the seasonal variability of particle phase formic acid.

Correlations	JST 2017 Summer	JST 2017 Winter	YRK 2016 Summer
Ca^{2+} vs $HCOO^-$	0.53	0.35	0.46
Mg^{2+} vs $HCOO^-$	0.35	0.66	0.52
K^+ vs $HCOO^-$	0.30	0.33	0.59
Ca^{2+} vs K^+	0.25	0.047	0.03
Ca^{2+} vs Mg^{2+}	0.53	0.037	0.74
K^+ vs Mg^{2+}	0.25	0.42	0.04
BrC vs K^+	0.57	0.66	N/A

In table (2) reasonably good correlations between formate and NVCs suggest a need to further investigate NVCs and their relationship with particle phase formic acid, including complexation between NVCs and formate.

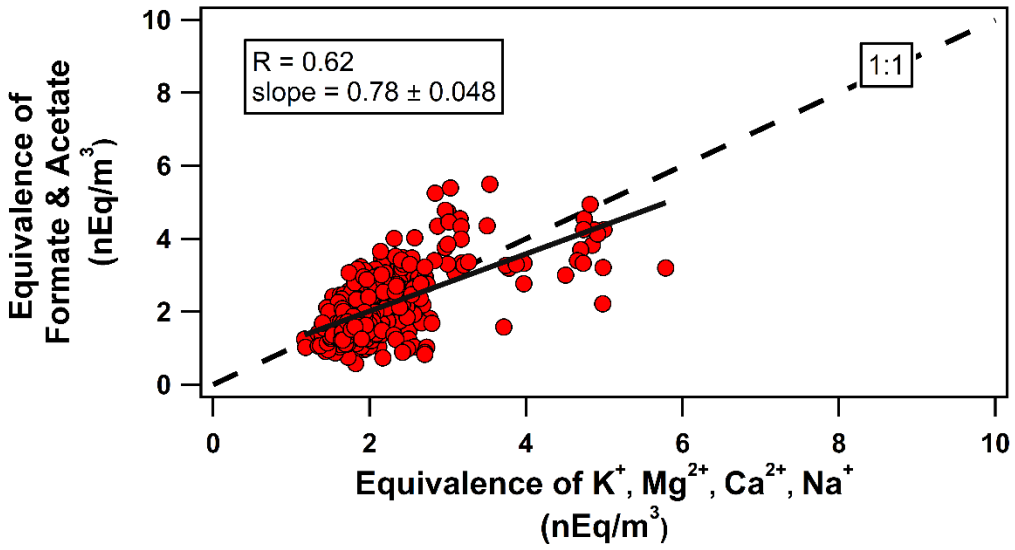

Figure 1: Yorkville, GA correlations between the sums of anions (formate and acetate) and cations (potassium, magnesium, calcium, and sodium) measured. Concentrations are shown in equivalence to compare positive and negative charges.

Figure (1) shows a scatter plot of the equivalence concentrations of formate plus acetate versus sum of the NVCs. Nano-equivalence (nEq/m^3) was obtained by converting the mass

concentrations (μg/m^3) of anions and cations $\left(\frac{\mu g}{m^3} \cdot \frac{mol}{g} \cdot \frac{g}{10^6 \mu g} \cdot \frac{10^9 nEq}{valence\ Eq} \cdot \frac{valence\ Eq}{1 mol} = \frac{nEq}{m^3}\right)$.

Figure (1) assesses whether there are enough cations to associate exclusively with formate and acetate to produce various salts (e.g., such as calcium formate, potassium formate, sodium formate, and magnesium formate). If the forms of these species was some combination of the various salts involving just these species, one would expect a slope of 1. The nano equivalence averages for NVCs, formate, and acetate are shown in table (3) for reference.

Table 3: Shown as average nano equivalence of cations and anions in both Yorkville and Atlanta.

Observed Compounds	**Average JST 2017 (nEq/m^3)**	**Average Yorkville 2016 (nEq/m^3)**
Ca^{2+}	6.19 ±4.80	1.96 ±0.90
Mg^{2+}	1.38 ±1.06	0.33 ±0.21
K^+	1.24 ±0.78	0.89 ±0.29
Na^+	N/A	0.47 ±0.37
Formate	0.57 ±0.40	1.16 ±0.52
Formate + Acetate	1.01 ±0.81	2.21 ±0.89

With a slope equal to 0.78 and R = 0.62, approximately half of the observations in figure (1) show that there are more formate and acetate ions available for bonding than total NVCs available, the cluster of data points above the 1:1 line and below show this separation. This division may be indicative of different physical processes that could be dominating formic acid partitioning, such as formate in high aerosol liquid water conditions or NVC complexation with formate.

In cases where there was sufficient NVC to associate with all the organic acids (points on or below the 1:1 line in figure (1)) the role of NVC complexation is investigated. Formic acid partitioning was predicted using equations (8-10) assuming internal mixture of all species (all

measured $PM_{1.0}$ anions and cations) and those analytical solutions (traces) are shown in figure (2).

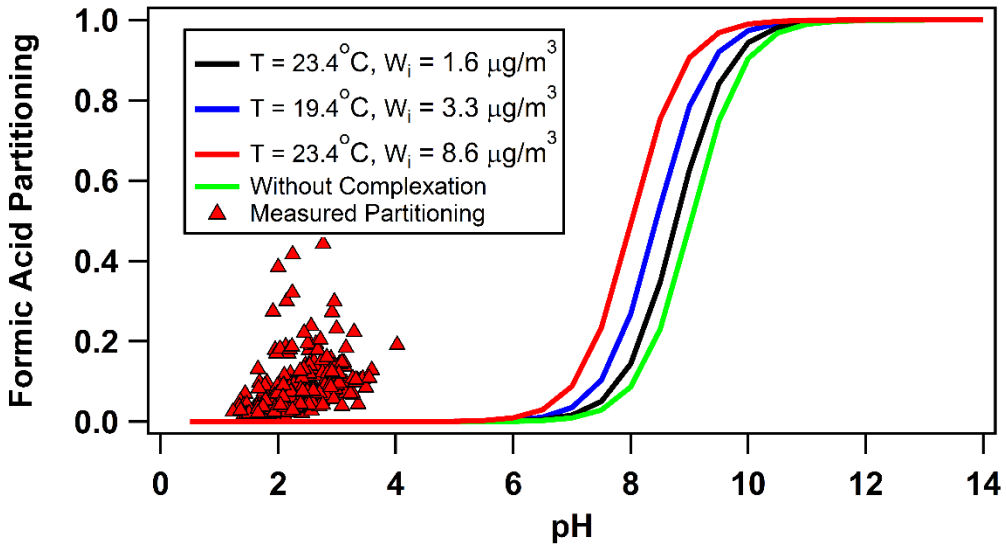

Figure 2: Measured partitioning of formic acid in Yorkville, GA and sigmoidal curves for formic acid complexation with K^+, Ca^{2+}, Mg^{2+}, and Na^+.

The pH was that determined by ISORROPIA assuming all inorganic species of $PM_{1.0}$ are internally mixed. This pH was used in the equations above to draw the traces in figure (2), and used with the ambient measurements of gas and particle formate to plot formic acid partitioning versus pH in figure (2). Initially, formic acid partitioning based on only Henry's law without any complexation was predicted and was consistent with predictions from Nah et al. (2018). For the analytical solution considering NVC complexation with formate we used the average W_i = 1.6 $\mu g/m^3$ determined by ISORROPIA II and the average ambient temperature = 23.4ºC. As shown in figure (2), it was found, similar to the findings of Nah et al. (2018), that there is still an underestimation of partitioning at low pH. W_i was increased to 8.6 $\mu g/m^3$, which is the upper limit for the predicted range of W_i and this shifted the sigmoidal curve the most, around 1.5 pH

units. However, this small shift in pH is not enough to resolve the disagreement between formic acid partitioning observed and predicted.

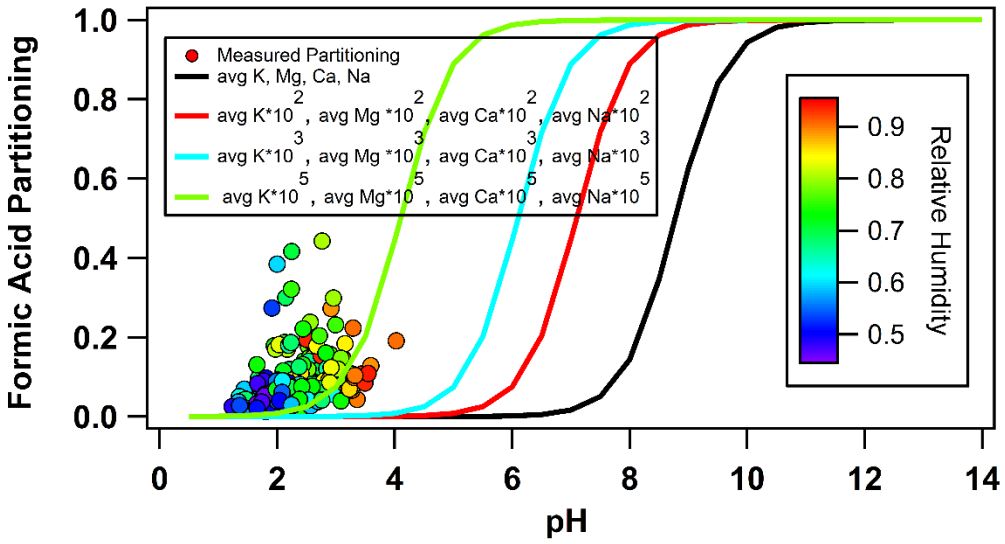

Figure 3: Measured partitioning from Yorkville, GA, multicolored markers show pH dependence on relative humidity. Analytical s-curves show formic acid complexation with K^+, Mg^{2+}, Ca^{2+}, and Na^+ at T = 23.4°C and W_i = 1.6 µg/m^3.

A sensitivity test was done by varying the average concentrations of NVCs to investigate formic acid partitioning behavior due to complexation with NVCs. The sigmoidal curves in figure (3) show that NVC concentrations can only produce some agreement with the measured partitioning of formic acid when the average concentrations of NVCs in the fine mode is over five order of magnitude greater than the ambient averages. Based on this, NVC complexation with formate is not a viable explanation for the observed particle formate at Yorkville assuming internal mixing.

3.2 JST Correlations and Nonvolatile Cation Complexation

An entire year of 24- hour filter measurements at JST in 2017 made it possible to investigate seasonal trends and behavior of formic acid. Seasonal trends for potassium, calcium, and formate

can be seen in figure (4), with higher concentrations in the winter months and on average lowest mass concentrations in the summer.

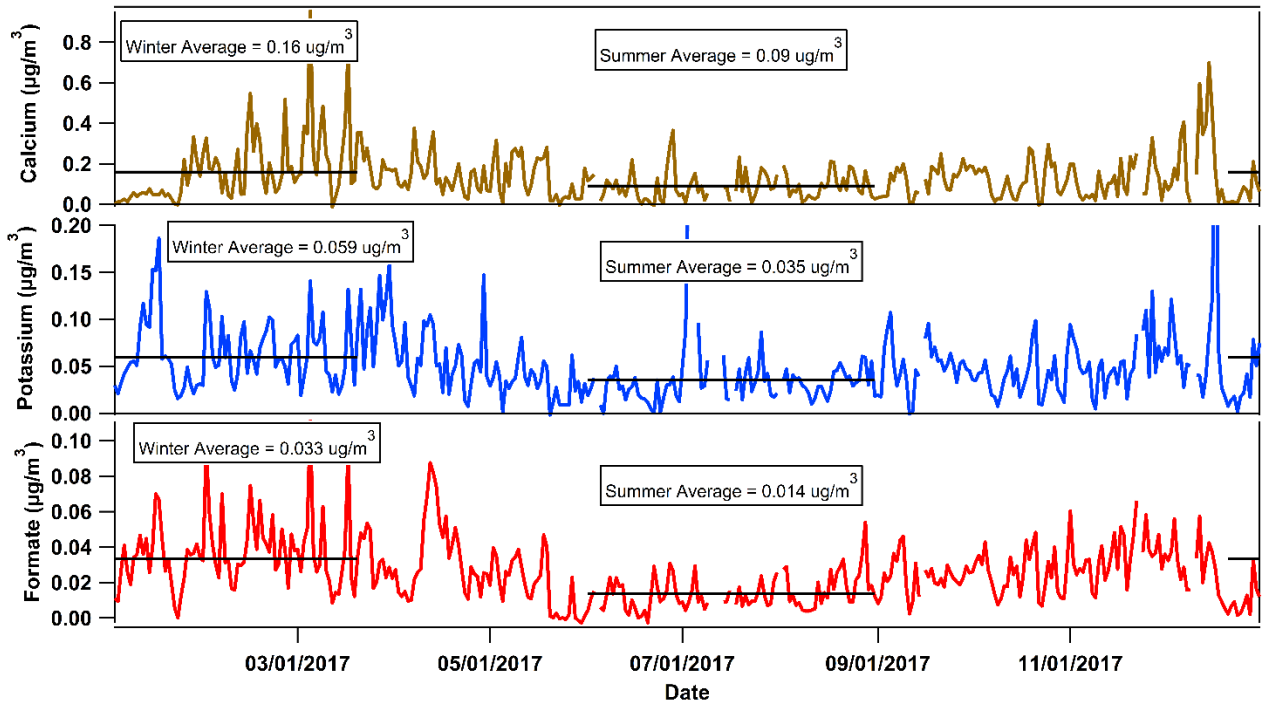

Figure 4: Time series of Jefferson Street $PM_{2.5}$ mass concentrations during 2017 are shown for potassium, calcium, and formate.

To test the hypothesis that winter and summer seasons were associated with statistically significant different mean mass concentrations of formate, calcium, and potassium, an independent samples t-test was performed. Based on the t-test, t_{calc} was equal to 3.57, 4.75, and 7.93 for calcium, potassium, and formate, respectively and all were greater than $t_{critical} = 1.98$ for 95% confidence with 120 degrees of freedom. Therefore, the null hypothesis could be rejected and it was concluded that there is a statistically significant difference between the mean mass concentrations of calcium, potassium, and formate in the winter and summer. Formic acid was expected to be higher in the summer, rather than the winter because a large source of formic acid is from photo chemical pathways [Veres et al. (2011)]. Even though formic acid production rates

might be higher in the summer than winter, its tendency to reside in the particle phase after it is formed is mainly controlled by the amount of liquid water in the particle. This is consistent with W_i obtained from ISOROPPIA II, which was higher in the winter ($W_i = 2.96 \pm 3.01$ μg/m^3) than the summer ($W_i = 2.22 \pm 1.44$ μg/m^3) .

The average mass concentration of Ca^{2+} measured in $PM_{2.5}$ at JST is approximately a factor of 6 higher than Ca^{2+} in $PM_{1.0}$ measured in Yorkville (Table (1)). In addition, the average mass concentration of Mg^{2+} in $PM_{2.5}$ at JST is a factor of 9 higher than the mass concentration of Mg^{2+} in $PM_{1.0}$ at Yorkville. The large differences in Mg^{2+} and Ca^{2+} between JST and Yorkville is likely due to the mineral dust associated with $PM_{2.5}$ at JST. The mass concentrations of potassium were not significantly different between $PM_{2.5}$ and $PM_{1.0}$ at JST and Yorkville, respectively, suggesting that a large fraction of K^+ resides in $PM_{1.0}$ at JST. Average $PM_{2.5}$ mass concentration at JST for formate was about a factor of 2 lower than the average $PM_{1.0}$ mass concentration of formate at Yorkville. Oxalate was the opposite, with JST $PM_{2.5}$ mass concentration about a factor of 2 larger than the Yorkville $PM_{1.0}$ mass concentration.

Good correlations can be observed in $PM_{2.5}$ filter samples from JST during 2017, as shown in Table (2). In the summer Ca^{2+} and $HCOO^-$ had an R = 0.53 and in the winter Mg^{2+} and $HCOO^-$ had an R = 0.66. Although the time resolution of the measurements is not as high as in Yorkville, the continuous year long filter data and the summer 2019 MOUDI measurements can help elucidate the mixing state and partitioning behavior of formic acid. In this section the NVCs are referring to Ca^{2+}, Mg^{2+}, and K^+, only. Na^+ was excluded because it was not measured. Also at JST, there was no acetate data available from the filters so acetate concentrations were assumed to be equal to the formate molar concentrations; previous studies around the Eastern United States have shown acetate and formate mass concentrations in the aerosol phase to be similar. In

Yorkville, GA Nah et al. (2018) reported $PM_{1.0}$ mass concentrations of formate equal to 0.05 ± 0.03 µg/m^3 and acetate equal to 0.06 ± 0.03 µg/m^3. Talbot et al. (1988) made measurements in eastern Virginia and reported $PM_{1.0}$ concentrations of formate and acetate as mixing ratios, mass concentrations were calculated and formate was equivalent to 0.028 ± 0.028 µg/m^3 and acetate was equivalent to 0.022 ± 0.020 µg/m^3.

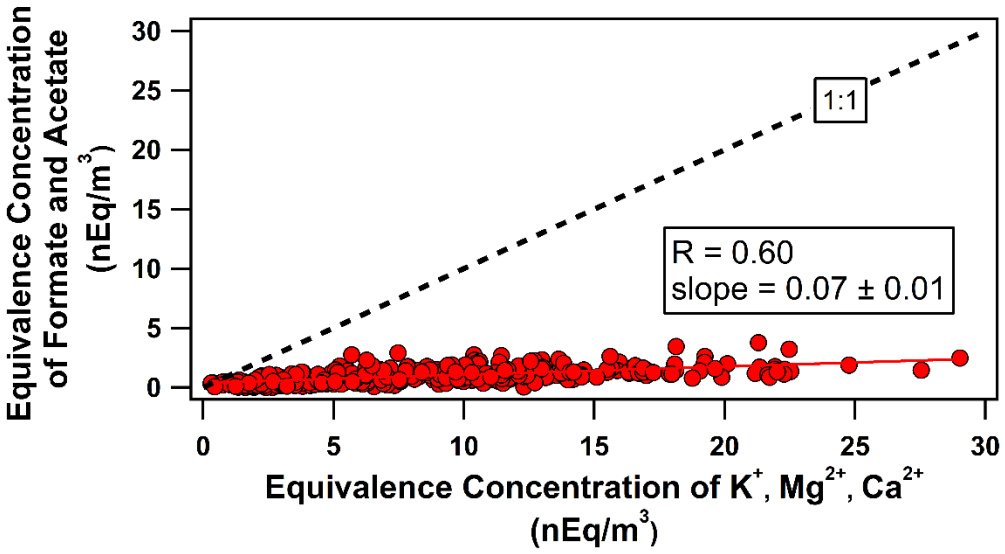

Figure 5: Jefferson Street formate and acetate correlated to NVCs (potassium, magnesium, and calcium). Sodium was not quantified, so it is not a part of the total NVC equivalence concentration.

Similar to the Yorkville analysis, the combined molar equivalence of formate and acetate were compared to the molar equivalence of NVCs in figure (5), which shows a good correlation (R = 0.60). The scatter plot shows an abundance of NVCs relative to formate and acetate, as indicated by the small slope of 0.07 ± 0.01. Therefore, it is possible that formate and acetate may, at all times, be in exclusively associated with just NVCs, such as through forming complexes. Oxalate may also be associated with some NVCs, but even with considering it, there are still excess NVC, as shown in figure (6). When including oxalate, the correlation drops (R =

0.33), suggesting that the association of formate and acetate with NVCs may be similar, but oxalate has less association.

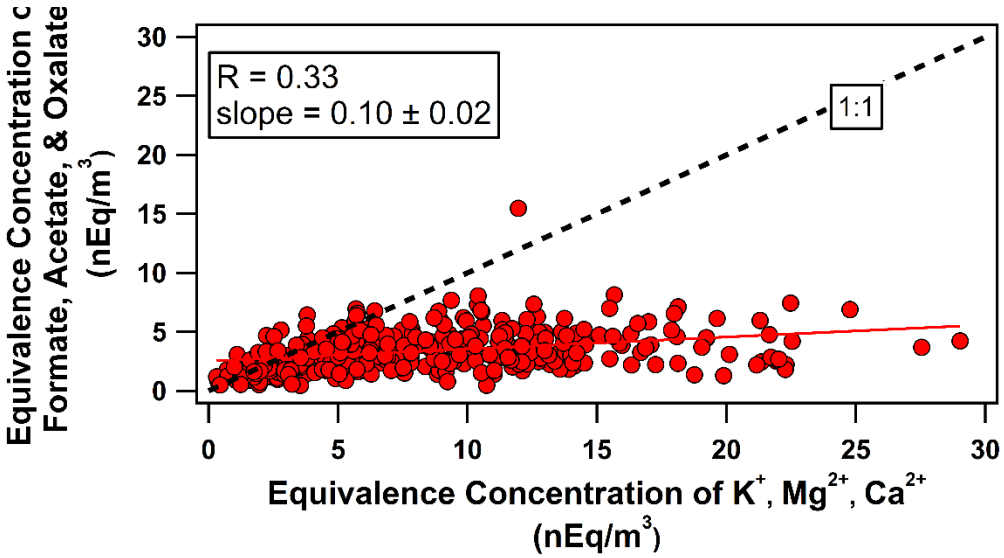

Figure 6: Jefferson Street acetate, formate, and oxalate correlated to NVCs (potassium, magnesium, and calcium).

$PM_{2.5}$ particle pH over the entire year was on average estimated to be 2.52 ± 1.3 pH units at JST. Average $PM_{2.5}$ bulk pH in the summer was the smallest at 1.89 ±0.42, while the winter season observed the largest average pH at 3.16 ±1.09. Also note that seasonal and annual bulk pH was determined in ISOROPPIA II running in reverse mode because inorganic gas phase data (ie. NH_3, HCl, HNO_3) was unavailable during most of the sampling period, with the exception of gas phase measurements in August 2017. Using the equations from section 2.6, the formic acid partitioning was predicted and shown as S-curves in figure (7) and compared to ambient data, where again the pH was determined by ISORROPIA assuming all species in $PM_{2.5}$ were internally mixed.

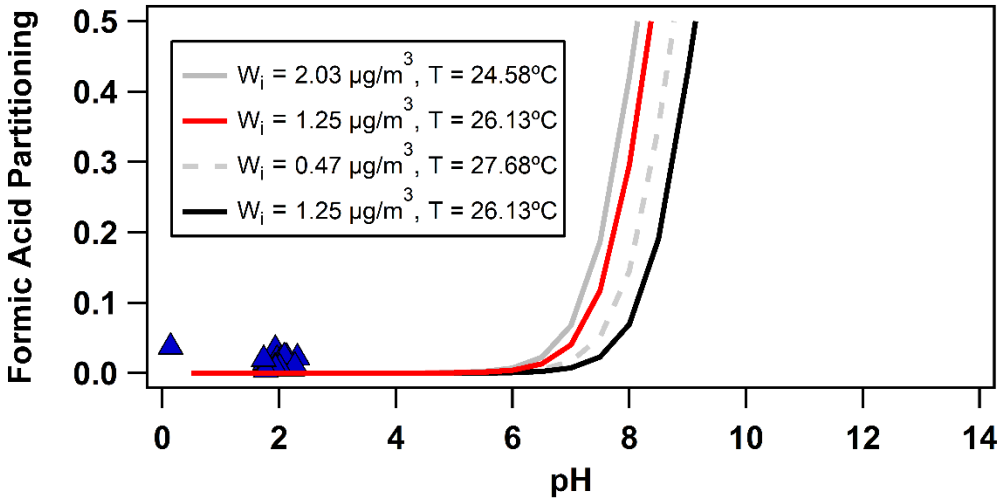

Figure 7: JST $PM_{2.5}$ bulk particle pH was calculated for August 2017. Red trace shows sigmoidal curve of partitioning when considering complexation with NVCs and black trace shows partitioning without the consideration of NVC complexation. Grey traces are S curves calculated using 1 standard deviation from average W_i and ambient temperature.

These results are only for the month of August 2017 because that was the only time gas phase formic acid measurements were available allowing the determination of measured formic acid partitioning. The results are similar to what was found in Yorkville. The observed partitioning of formic acid was small, the average value of $\varepsilon(CHOO^-)$ was 0.014 and in many cases close to 0.001, but the predicted partitioning was always very low at pH < 5. In figure (7), the black trace is the analytical solution for formic acid partitioning without the consideration of NVC complexation. The red trace shows partitioning of formic acid with complexation effects using average W_i = 1.25 µg/m^3 and average ambient temperature = 26.13°C . The grey traces are S curves calculated using 1 standard deviation from the average W_i and ambient temperature. At pH ranges from 0 to 5.5, there is essentially no partitioning to condensed phase predicted, however; formic acid partitioning is observed in small amounts around a pH of 2.

3.3 Georgia Tech MOUDI Size Distributions

While the previous analysis was based on bulk measurements of aerosol composition (e.g. $PM_{1.0}$ or $PM_{2.5}$), measurements of aerosol size resolved composition can provide more insights on the partitioning of formic acid, such as possible mixing states of NVCs and organic acids. Figure 8a shows chemically resolved size distributions. Formate was observed to have 2 modes in the size distribution, one mode is less than 1.0 μm and the second mode is greater than 1.0 μm and continues on into the coarse mode. This is also shown in figure 8b as well. Figure 8c and 8d show the tail of formate distribution in the coarse mode (>2.5 μm). Oxalate also has two peaks in its distributions, based on four measurement periods the smaller peak is always collocated with the formate peak in the same size range (0.18 – 0.32 μm). This may suggest that formate and oxalate have similar sources. Ammonium and sulfate are largely secondary species and are found mainly in the fine mode; here they have distributions observed with single modes with average peak diameters of 0.30 and 0.32 μm, respectively. As seen in all four MOUDI measurements, mineral dust species, such as magnesium and calcium each have single modes that generally peak in the coarse mode, but with a tail down to 1 μm. Like mineral dust, sodium typically showed single mode distributions that peaked in the coarse mode range with a tail into the fine mode, with the exception of figure 8a where sodium has a bimodal distribution, suggesting different sources of sodium other than mineral dust and sea salt. (Note that there is some uncertainty in Na^+ data since contamination may have been an issue). As shown in figure 8a, 8b, and 8d, potassium has a bimodal distribution, one mode is in the fine mode while the second mode is usually in the coarse mode, this is consistent with two possible sources for K^+ , biomass burning which is known to produce fine mode K^+ [Metzger et al. (2006), Li et al.

(2003), Andreae et al. (1983)] and mineral dust and sea salt mainly found in the coarse mode contains K^+[Metzger et al. (2006), Li et al. (2003), Zhang et al. (2010), Cruz et al. (2019)].

The bimodal size distributions of formate (and oxalate) suggest it may be associated with different aerosol components, depending on particle size. In the coarse mode, based on the size distributions, formate and oxalate could have associations with coarse mode aerosol species such as sodium, potassium, magnesium, and calcium, which could be from mineral dust and sea salt. In addition, formate and oxalate could have associations with fine mode aerosol species such as ammonium and sulfate and/or potassium. Studies with Reid et al. (1998) showed that ammonium is strongly correlated to oxalate and other organic species in regions dominated by biomass burning. We will assume that the ambient size distributions obtained at Georgia Tech are representative of the air masses sampled in Yorkville and JST.

In Yorkville and JST, the assumption was made that the observed aerosols were internally mixed in a bulk mixture and so bulk pH was determined from ISORROPIA II based on all $PM_{1.0}$ or $PM_{2.5}$ components all mixed together. A limitation of this bulk pH assumption is that it ignores the influence of particle size on aerosol pH. Using the Atlanta MOUDI measurements to calculate the particle pH assuming internal mixing at each impactor stage could show the pH dependence on particle size. Size resolved particle pH was calculated from the four MOUDI measurements described in figure (8) and averaged, as shown in figure (9).

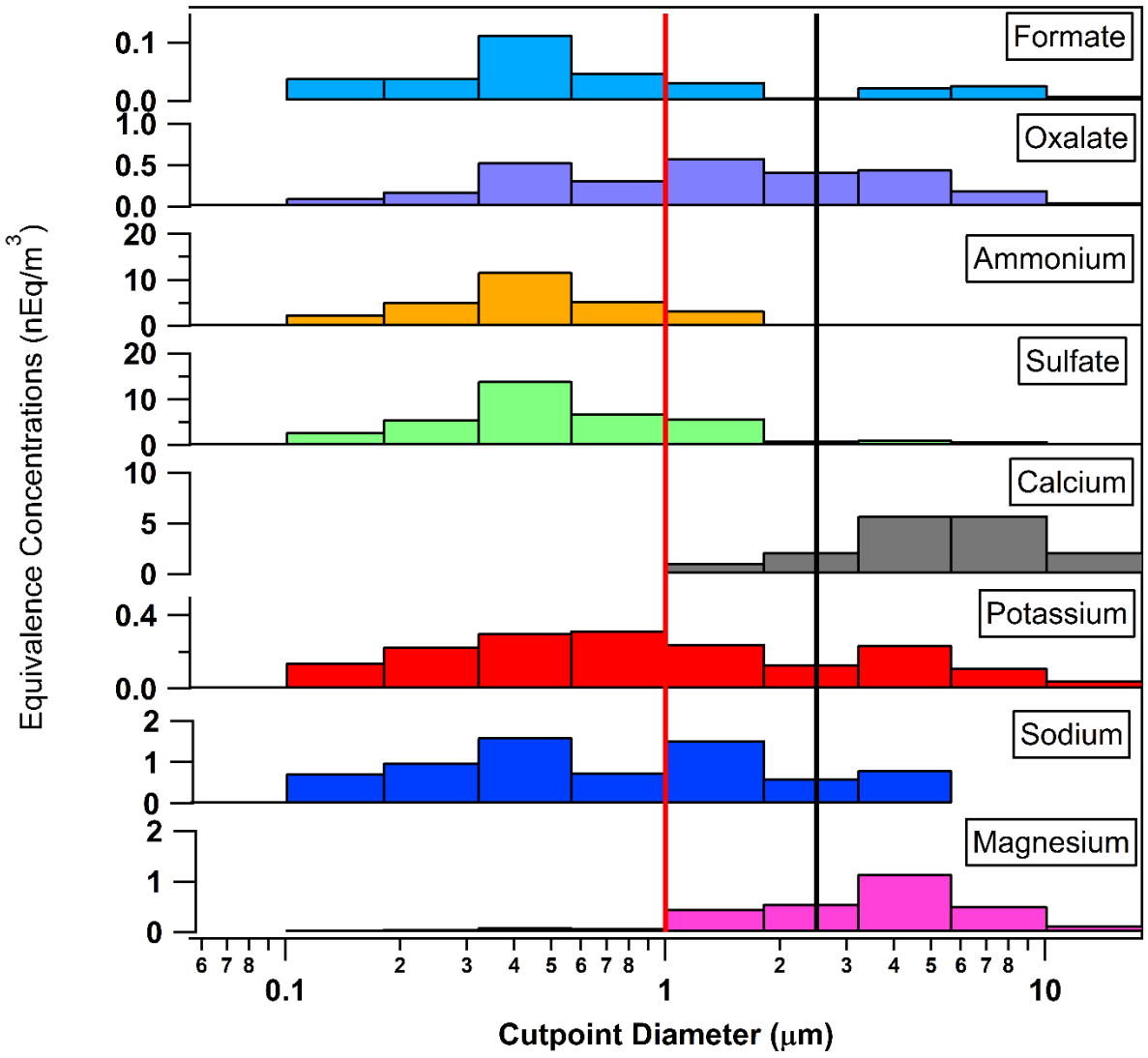

Figure 8a: MOUDI measurements from Atlanta during May 14 – 21, 2019 with size distributions of formate, oxalate, ammonium, sulfate, calcium, sodium, magnesium, and potassium. The black line and red line is used to identify the cutoff for $PM_{2.5}$ and $PM_{1.0}$, respectively.

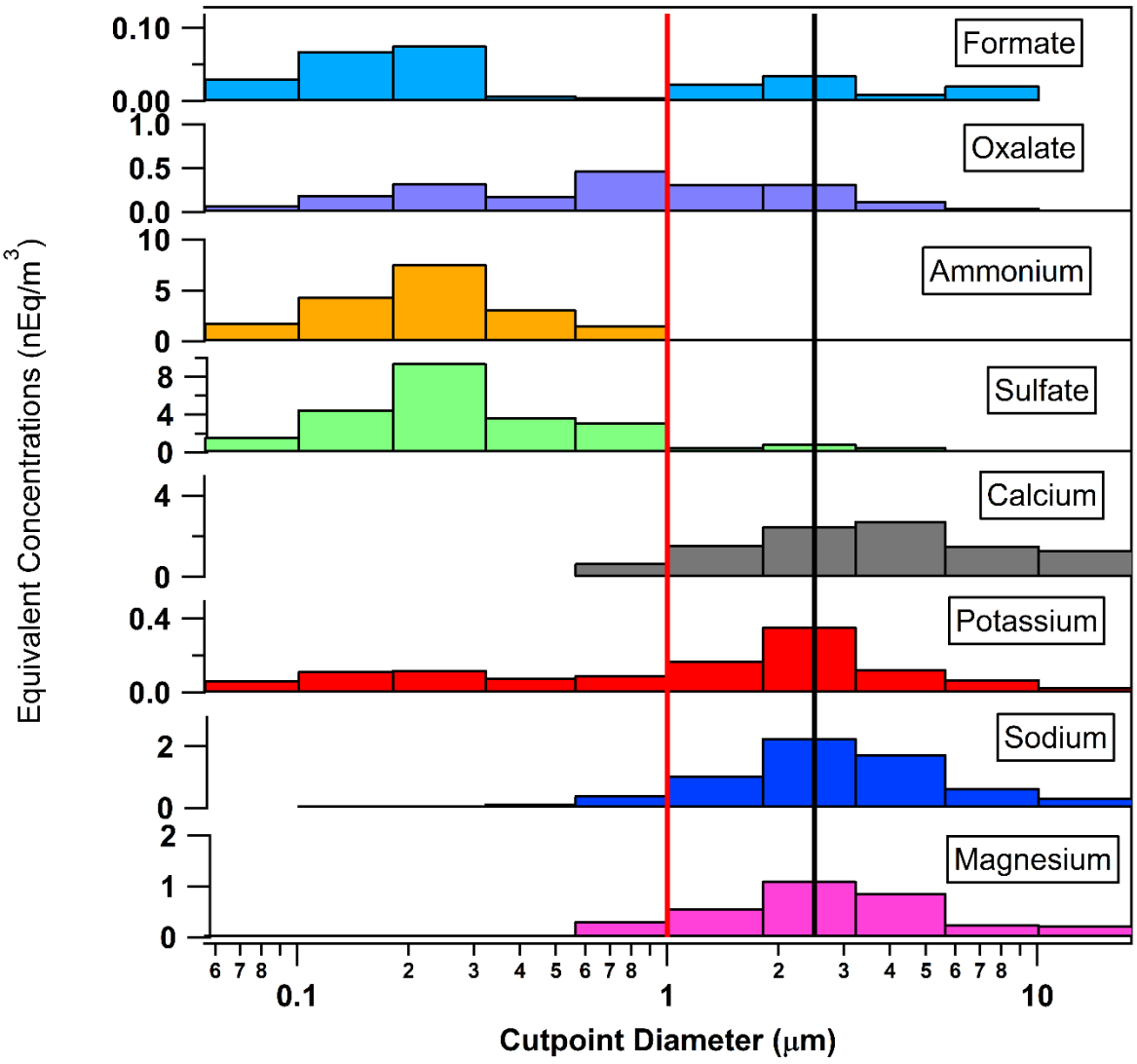

Figure 8b: Sampling period, June 10 –17, 2019.

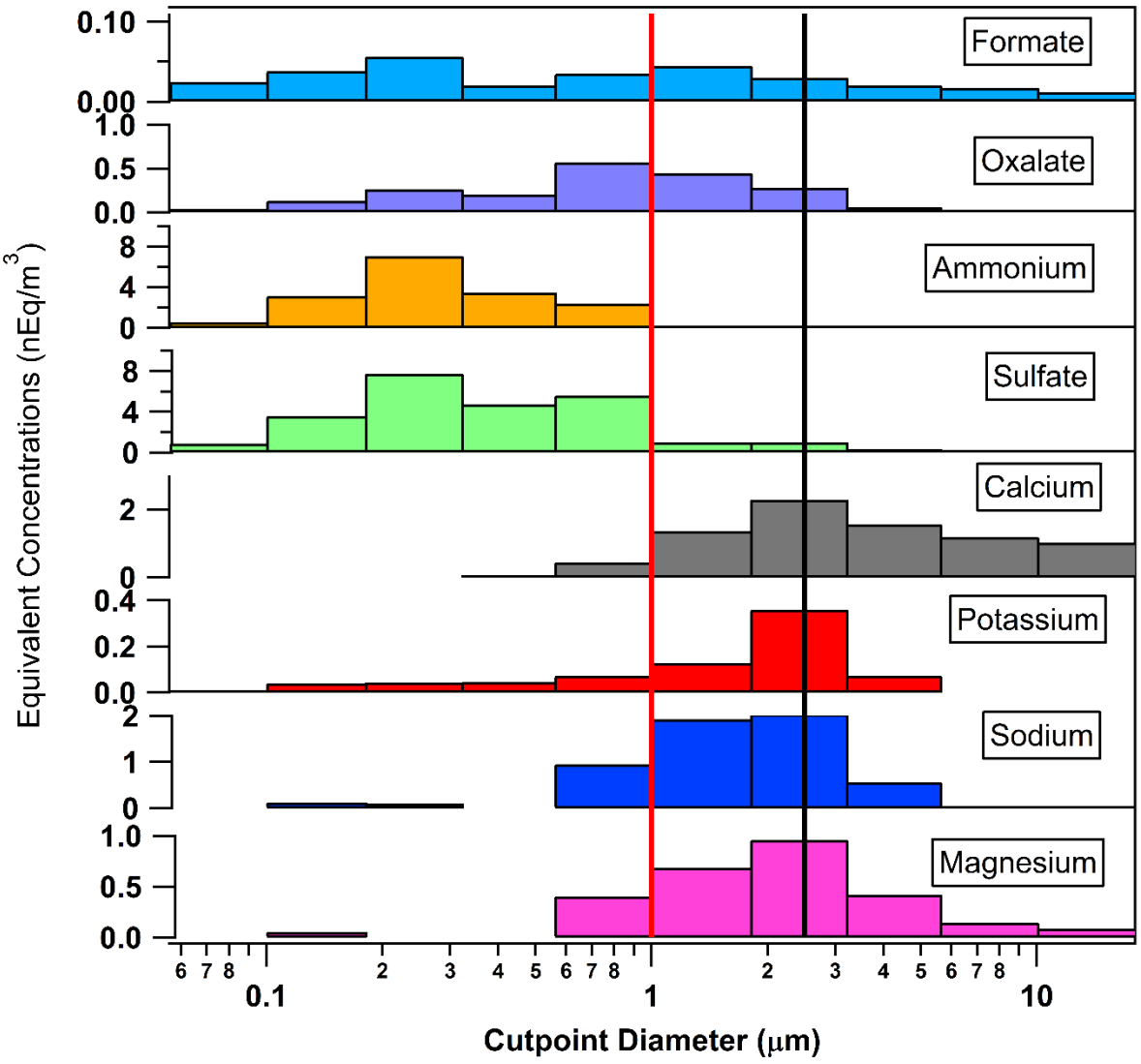

Figure 8c: Sampling period, July 17 – 24, 2019.

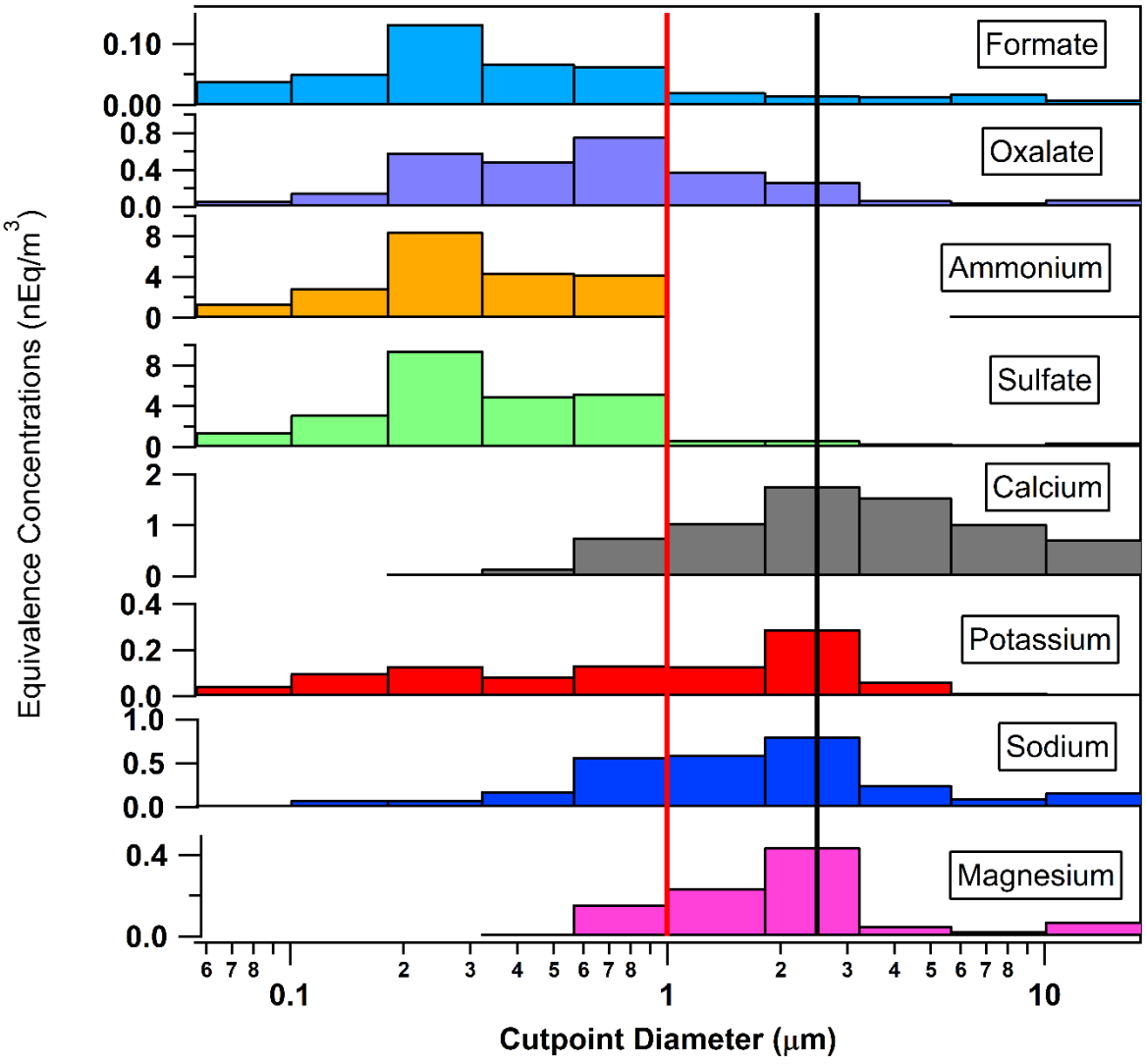

Figure 8d: Sampling period, July 30 – Aug 06, 2019.

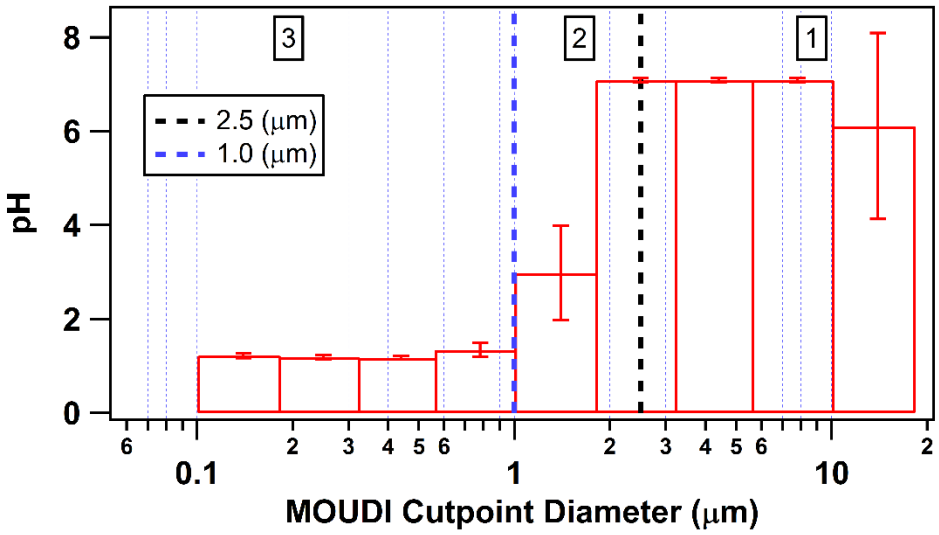

Figure 9: Average pH for each MOUDI stage was calculated using ISORROPIA II and plotted as a function of MOUDI stage cutpoint diameter.

Figure (9) can be divided into three regimes based on pH: (1) diameters greater than 2.5 μm ($PM_{2.5-10}$), (2) diameters between 1.0 and 2.5 μm ($PM_{1-2.5}$) and (3) diameters less than 1.0 μm (PM_1). The average pH of regime 1 is 6.9, the higher pH is due to the dominance of NVCs and little sulfate. Regime 2 is a transition region between the other two size regimes, it shows the most range in pH because sulfate contributes to the lowering of bulk particle pH, the tail of sulfate distributions entering regime 2 and the NVC in this regime raise pH, as can be seen in figures (8a-8d). In regime 3 the average pH was 1.2 which was being driven by high concentrations of sulfate.

3.4 Yorkville $PM_{1.0}$ Discussion

In section 3.1 it was shown that at Yorkville, $PM_{1.0}$ formic acid complexation with NVCs could not explain the discrepancy between the observed and predicted partitioning of formic acid. Furthermore, the size distributions suggest that there is little Ca^{2+}, Mg^{2+}, and Na^{+} in this

$PM_{1.0}$ size range, leaving K^+ as likely the main NVC that could affect $PM_{1.0}$ formate. For $PM_{1.0}$, the bulk particle pH remains too low with the assumption of an internal mixing state because of the strong influence of sulfate and its hydroscopicity. Since the average bulk pH of aerosols in Yorkville and JST are similar, 1.88 ± 0.76 and 2.52 ± 1.3, respectively, we will use Georgia Tech MOUDI results to speculate on what may drive partitioning behavior in both Yorkville and JST. Based on MOUDI measurements, the pH dependence on particle size for $PM_{1.0}$ is not significant. Figure 12 highlights this in region 3, the pH is low and does not fluctuate significantly. In addition, the filter stages below 1.0 μm are dominated by sulfate and lack a large amount of cations necessary to raise the bulk pH. Interestingly, the formate peak in the fine mode coincides with K+ in the fine mode and equivalent concentration comparisons indicate that formate ions can be balanced by the potassium ions. In Yorkville, the good correlation between the K^+ and $HCOO^-$ (R = 0.59) suggests that they may be associated. Also the nanoequivalence comparison in table (3) between K^+ and $CHOO^-$ show that within the standard deviations the potassium and formate charges could balance each other. One way that formate could be observed in the fine mode is if it was associated with K^+ and these species were externally mixed with most of the other aerosol in that size range, that is ammonium sulfate (and likely organic species, which were not measured). This would only be likely if they were measured nearby its source. However, in this study it was not possible to identify the source of formic acid and potassium.

Previous source apportionment studies using Positive Matrix Factorization (PMF) have reported on water-soluble K^+ in $PM_{2.5}$ in the southeast. The $PM_{2.5}$ mass source contributions attributed 43%, 18%, 16%, and 22% of K^+ to refractory material, residual, biomass burning, and secondary aerosols, respectively (Zhang et al., 2010). If we were to assume some external mixting for K^+ and $CHOO^-$, then $CHOO^-$ would most likely be associated with the PMF factor

for refractory material, such as mineral dust. Mineral dust is commonly connected to refractory materials and the often large excess of NVCs in mineral dust size mode can provide neutral pH conditions for formic acid partitioning. However, with $PM_{1.0}$ in Yorkville there will probably be a lack of NVCs to raise pH if mixed with sulfate, as would be expected for more aged aerosol and based on the size distributions of NVCs and sulfate. Secondary aerosols would most likely have low pH because they would have long enough lifetimes to become acidic and coagulate with sulfate particles. An external mixture of K^+ and $CHOO^-$ (with brown carbon (BrC) as a tracer for biomass burning) would also be unlikely unless very close to the source. Lastly, there is still about 18% of residual (unmeasured species) material associated with K^+, which would have contributions from elemental carbon and water-insoluble organic species (Zhang et al., 2010). The residual material if freshly emitted could have a particle pH close to neutral, which could meet the conditions for observed particle phase formic acid, but an exact explanation requires further research. Also, Zhang et al. (2010) did source apportionment of $PM_{2.5}$, so there may be some differences with $PM_{1.0}$ such as K^+ associated with refractory material having a smaller source contribution and biomass burning being relatively larger. Even though the good correlations between $CHOO^-$ with K^+ , Mg^{2+}, and Ca^{2+} suggest mineral dust associations, there is not enough evidence to show that an external mixture exists.

3.5 Jefferson Street $PM_{2.5}$ Discussion

It was shown in section 3.2 that measured formic acid partitioning at times was greater than zero and so did not agree with the predicted partitioning shown by the S curves and markers in figure (7). Since both JST and MOUDI measurements were taken in Atlanta, here we assume that $PM_{2.5}$ measured at JST has a size distribution characterized by Georgia Tech MOUDI measurements, despite different time periods. JST's main difference from Yorkville was that it

had an abundance of NVCs as shown in table (3), most likely due to nearby anthropogenic sources, such as construction sites that raise dust (ie. larger Ca^{2+} and Mg^{2+} in JST, Table (3)). In addition, JST samples measured $PM_{2.5}$ and based on the MOUDI size distributions there is a large contribution of NVCs in between 1.0 to 3.2 μm. Formate is also observed on filter stages between 1.0 to 3.2 μm. Assuming internal mixing for each MOUDI stage, figure (9) indicates that particle pH in between 1.0 to 3.2 μm has a large range (3 to 7). In region 2, pH dependence on size is important because there is a small amount of sulfate relative to NVC concentrations. As a result, pH between 1.0 to 2.5 μm can be neutral or acidic and formic acid partitioning at JST may occur due to complexation with NVCs at the near neutral pH of the upper end of the $PM_{1\text{-}2.5}$ range. To understand the pH of particles between 1.0 to 3.2 μm the particle mass less than 1.0 μm MOUDI stages was subtracted from particle mass less than 3.2 μm MOUDI stages for sulfate, formate, sodium, ammonium, calcium, potassium, and magnesium and divided by the total mass below 3.2 μm. 3.2 μm is used instead of 2.5 μm because the MOUDI impactor stage was designed for 3.2 μm cutsize. On average, the mass concentration between 1.0 to 3.2 μm was 9.55% (SO_4^{2-}), 17.49% ($CHOO^-$), 61.26% (Na^+), 3.09% (NH_4^+) , 85.81% (Ca^{2+}) , 45.17% (K^+), 78.23% (Mg^{2+}), 54.84% (NO_3^-), and 21.43% (Cl^-) of the total $PM_{2.5}$ measured mass. NO_3^- and Cl^- fractions between 1.0 to 3.2 μm were obtained from results in Fang et al. (2017). By assuming an internal mixture for cut sizes between 1.0 to 3.2 μm, the observed formate partitioning could be explained by the neutral pH as seen in figure (10). At an average pH unit of 7.06, the observed formate had $\varepsilon(CHOO^-)$ between 0.0040 and 0.037 showing better agreement with the predicted s-curves which around pH 7 had a $\varepsilon\ (CHOO^-)$ range from 0.0074 to 0.068.

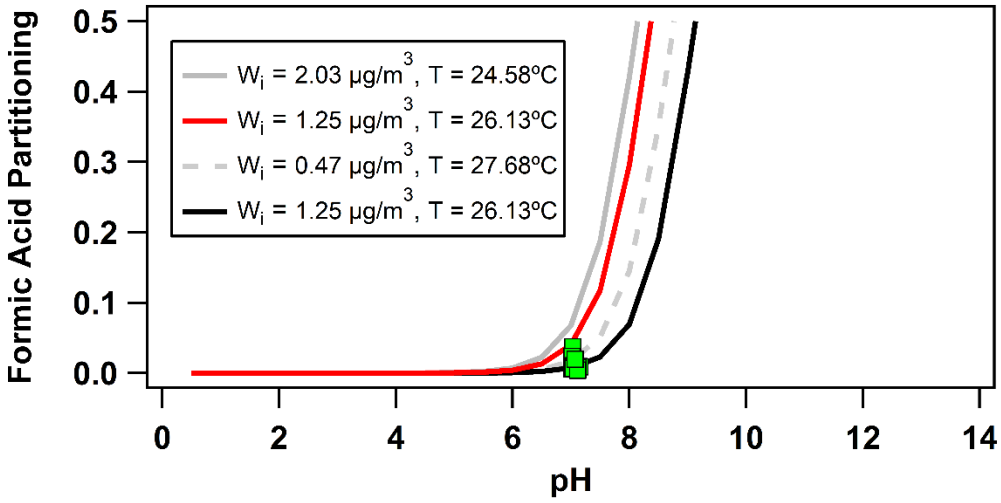

Figure 10: New bulk particle pH (green markers) with external mixing assumption for particles 1.0 to 2.5 µm.

Although formic acid partitioning could be explained by neutral pH between 1 to 2.5 µm, at cut sizes less than 1.0 µm formic acid partitioning issues are the same as for the Yorkville $PM_{1.0}$ case, it cannot be explained in the same way because the pH is too low and the particles likely internally mixed since aged, and there is not enough NVCs. Approximately 82% of the formic acid mass is still in the fine mode as estimated in size distributions, but it still remains unclear how formic acid behaves in this region. The strongest correlation observed at JST in the summer was between $CHOO^-$ and Ca^{2+} (R = 0.53) which suggests some association with mineral dust possibly driven by the Ca^{2+} at the higher end of the $PM_{2.5}$ range. In the winter season Mg^{2+} has the highest correlation with $CHOO^-$ (R = 0.66) indicating different sources could contribute to formic acid partitioning.

CHAPTER 4

CONCLUSIONS AND FUTURE WORK

4.1 Summary

This thesis investigates the partitioning of formic acid between gas and particle phases based on data from three measurement sites in the state of Georgia. Correlations between NVCs and formic acid indicate different sources may contribute to formic acid partitioning in Yorkville and Atlanta, GA. In Yorkville, formate was well correlated to K^+, Mg^{2+}, and Ca^{2+} which suggested possible sources of formic acid associated with mineral dust and biomass burning. In JST, the good formate correlations to Ca^{2+} and Mg^{2+} also suggested that formic acid could be associated with mineral dust contributions to $PM_{2.5}$ throughout the year. The results were also used to investigate formic acid partitioning behavior and to possibly provide additional insight to answer the question for why observed formic acid partitioning disagreed with predicted partitioning behavior based on bulk analysis of fine PM. It was shown that assuming $PM_{1.0\text{-}2.5}$ was externally mixed from $PM_{1.0}$ at JST improved the agreement between the measured and predicted formic acid partitioning because the partitioning pH was closer to neutral. Although NVC complexation could explain observed formic acid partitioning in the 1.0 to 2.5 μm range, as shown in JST, it could not resolve the disagreement with particles less than 1.0 μm. This suggests that there may be different chemical processes and sources of formic acid that may be contributing to the fine and coarse mode. Another possible reason is that formic acid is being freshly emitted and therefore is not entirely in an internal mixture, the extent of the fine particle mixing is unclear.

4.2 Future Work

Even though ISORROPIA-II can predict bulk particle pH reasonably well, the bulk particle pH assumption still cannot explain formic acid partitioning behavior in $PM_{1.0}$. Since ISORROPIA II neglects organic ions as inputs and because aqueous phase aerosols may be externally mixed to some extent, there is a need to look into single particle measurements rather than bulk measurements. Furthermore, it is necessary to investigate whether semi-volatile organics such as formic and acetic acid agree with the assumption of gas-particle equilibrium. Two studies that would help elucidate the partitioning of formic acid in the fine mode would be to investigate the mixing state of PM and understand the source of formic acid sampled at measurement sites. Source apportionment using PMF analysis for JST and Yorkville could help to determine what kind of source factors are associated with formic acid and NVCs. Single particle analysis, for example; using the particle analysis by laser spectrometry (PALMS) would be a valuable tool to investigate particle mixing state. Methods for quantifying aerosol mixing from single particle measurements are highlighted by Riemer and West (2013) and Bondy et al. (2018), using mixing state indices for different particle classes.

REFERENCES

Alwe, H. D., D. B. Millet, X. Chen, J. D. Raff, Z. C. Payne, and K. Fledderman (2019, March). Oxidation of Volatile Organic Compounds as the Major Source of Formic Acid in a Mixed Forest Canopy. *Geophysical Research Letters 46*(5), 2940–2948.

Andreae, M. O. (1983). Soot carbon and excess fine potassium: Long-range transport of combustion-derived aerosols. *Science 220*(4602), 1148–1151.

Bondy, A. L., D. Bonanno, R. C. Moffet, B. Wang, A. Laskin, and A. P. Ault (2018). The diverse chemical mixing state of aerosol particles in the southeastern united states. *Atmospheric Chemistry and Physics (Online) 18*(PNNL-SA-138963).

Bunting, J. W. and K. M. Thong (1970). Stability constants for some 1: 1 metal–carboxylate complexes. *Canadian Journal of Chemistry 48*(11), 1654–1656.

Chaliyakunnel, S., D. Millet, K. Wells, K. Cady-Pereira, and M. Shephard (2016). A large underestimate of formic acid from tropical fires: constraints from space-borne measurements. *Environmental Science & Technology 50*(11), 5631–5640.

Cruz, M. T., P. A. Bañaga, G. Betito, R. A. Braun, C. Stahl, M. A. Aghdam, M. O. Cambaliza, H. Dadashazar, M. R. Hilario, G. R. Lorenzo, et al. (2019). Size-resolved composition and morphology of particulate matter during the southwest monsoon in metro manila, philippines.

Fang, T., H. Guo, L. Zeng, V. Verma, A. Nenes, and R. J. Weber (2017). Highly acidic ambient particles, soluble metals, and oxidative potential: a link between sulfate and aerosol toxicity. *Environmental science & technology 51*(5), 2611–2620.

Fountoukis, C. and A. Nenes (2007). Isorropia II: a computationally efficient thermodynamic equilibrium model for K^+, Ca^{2+}, Mg^{2+}, NH_4^+, Na^+, SO_4^{2-}, NO_3^-, Cl^-, H_2O aerosols.

Gao, D., K. J. Godri Pollitt, J. A. Mulholland, A. G. Russell, and R. J. Weber (2020). Characterization and comparison of pm2. 5 oxidative potential assessed by two acellular assays. *Atmospheric Chemistry & Physics 20*(9).

Gao, D., J. A. Mulholland, A. G. Russell, and R. J. Weber (2020). Characterization of water-insoluble oxidative potential of $PM_{2.5}$ using the dithiothreitol assay. *Atmospheric Environment 224*, 117327.

Goode, J. G., R. J. Yokelson, D. E. Ward, R. A. Susott, R. E. Babbitt, M. A. Davies, and W.M. Hao (2000). Measurements of excess o3, co2, co, ch4, c2h4, c2h2, hcn, no, nh3, hcooh, ch3cooh, hcho, and ch3oh in 1997 alaskan biomass burning plumes by airborne fourier transform infrared spectroscopy (aftir). *Journal of Geophysical Research: Atmospheres 105*(D17), 22147–22166.

Gordon, H., J. Kirkby, U. Baltensperger, F. Bianchi, M. Breitenlechner, J. Curtius, A. Dias, J. Dommen, N. M. Donahue, E. M. Dunne, et al. (2017). Causes and importance of new particle formation in the present-day and preindustrial atmospheres. *Journal of Geophysical Research: Atmospheres 122*(16), 8739–8760.

Guo, H., A. Nenes, and R. J. Weber (2017). The underappreciated role of nonvolatile cations on aerosol ammonium-sulfate molar ratios. *Atmos Chem Phys Discuss. 2017b https://doi. org/10.5194/acp-2017-737*.

Guo, H., A. P. Sullivan, P. Campuzano-Jost, J. C. Schroder, F. D. Lopez-Hilfiker, J. E. Dibb, J. L. Jimenez, J. A. Thornton, S. S. Brown, A. Nenes, et al. (2016). Fine particle pH and the partitioning of nitric acid during winter in the northeastern united states. *Journal of Geophysical Research: Atmospheres 121*(17), 10–355.

Guo, H., L. Xu, A. Bougiatioti, K. M. Cerully, S. L. Capps, J. Hite Jr, A. Carlton, S.-H. Lee, M. Bergin, N. Ng, et al. (2015). Fine-particle water and pH in the southeastern united states. *Atmospheric Chemistry & Physics 15*(9).

Hansen, D. A., E. S. Edgerton, B. E. Hartsell, J. J. Jansen, N. Kandasamy, G. M. Hidy, and C. L. Blanchard (2003). The southeastern aerosol research and characterization study: part 1—overview. *Journal of the Air & Waste Management Association 53*(12), 1460–1471.

Heintzenberg, J. (1989). Fine particles in the global troposphere a review. *Tellus B 41*(2), 149–160.

Hiller, F. W. (1966). A study of the iodine-formate reaction in dimethylsulfoxide-water mixtures.

Keene, W. C., A. A. Pszenny, J. R. Maben, E. Stevenson, and A. Wall (2004). Closure evaluation of size-resolved aerosol ph in the new england coastal atmosphere during summer. *Journal of Geophysical Research: Atmospheres 109*(D23).

Keene, W. C., R. Sander, A. A. Pszenny, R. Vogt, P. J. Crutzen, and J. N. Galloway (1998). Aerosol ph in the marine boundary layer: A review and model evaluation. *Journal of Aerosol Science 29*(3), 339–356.

Khare, P., N. Kumar, K. M. Kumari, and S. S. Srivastava (1999, May). Atmospheric formic and acetic acids: An overview. *Reviews of Geophysics 37*(2), 227–248.

Li, J., M. Pósfai, P. V. Hobbs, and P. R. Buseck (2003). Individual aerosol particles from biomass burning in southern africa: 2, compositions and aging of inorganic particles. *Journal of Geophysical Research: Atmospheres 108*(D13).

Lim, Y., Y. Tan, M. Perri, S. Seitzinger, and B. Turpin (2010). Aqueous chemistry and its

role in secondary organic aerosol (soa) formation. *Atmospheric Chemistry & Physics Discussions 10*(6).

Liu, J., X. Zhang, E. T. Parker, P. R. Veres, J. M. Roberts, J. A. de Gouw, P. L. Hayes, J. L. Jimenez, J. G. Murphy, R. A. Ellis, L. G. Huey, and R. J. Weber (2012, November). On the gas-particle partitioning of soluble organic aerosol in two urban atmospheres with contrasting emissions: 2. Gas and particle phase formic acid: Formic Acid Partitioning In Los Angeles and Atlanta. *Journal of Geophysical Research: Atmospheres 117*(D21), n/a–n/a.

Marple, V. A., K. L. Rubow, and S. M. Behm (1991). A microorifice uniform deposit impactor (moudi): Description, calibration, and use. *Aerosol Science and Technology 14*(4), 434–446.

McNeill, V. F. (2015). Aqueous organic chemistry in the atmosphere: Sources and chemical processing of organic aerosols.

Meskhidze, N., W. Chameides, A. Nenes, and G. Chen (2003). Iron mobilization in mineral dust: Can anthropogenic so2 emissions affect ocean productivity? *Geophysical Research Letters 30*(21).

Metzger, S., N. Mihalopoulos, and J. Lelieveld (2006). Importance of mineral cations and organics in gas-aerosol partitioning of reactive nitrogen compounds: case study based on minos results.

Millet, D. B., M. Baasandorj, D. K. Farmer, J. A. Thornton, K. Baumann, P. Brophy, S. Chaliyakunnel, J. A. de Gouw, M. Graus, L. Hu, A. Koss, B. H. Lee, F. D. Lopez-Hilfiker, J. A. Neuman, F. Paulot, J. Peischl, I. B. Pollack, T. B. Ryerson, C. Warneke, B. J. Williams, and J. Xu (2015, June). A large and ubiquitous source of atmospheric formic acid. *Atmospheric Chemistry and Physics 15*(11), 6283–6304.

Mungall, E. L., J. P. Abbatt, J. J. Wentzell, G. R. Wentworth, J. G. Murphy, D. Kunkel, E. Gute, D. W. Tarasick, S. Sharma, C. J. Cox, et al. (2018). High gas-phase mixing ratios of formic and acetic acid in the high arctic. *Atmospheric Chemistry and Physics 18*(14), 10237–10254.

Nah, T., H. Guo, A. P. Sullivan, Y. Chen, D. J. Tanner, A. Nenes, A. Russell, N. L. Ng, L. G. Huey, and R. J. Weber (2018, August). Characterization of aerosol composition, aerosol acidity, and organic acid partitioning at an agriculturally intensive rural southeastern US site. *Atmospheric Chemistry and Physics 18*(15), 11471–11491.

Nah, T., Y. Ji, D. J. Tanner, H. Guo, A. P. Sullivan, N. L. Ng, R. J. Weber, and L. G. Huey (2018, September). Real-time measurements of gas-phase organic acids using SF_6^- chemical ionization mass spectrometry. *Atmospheric Measurement Techniques* 11(9), 5087–5104.

National Academies of Sciences, E., Medicine, et al. (2016). *The future of atmospheric chemistry research: remembering yesterday, understanding today, anticipating tomorrow*. National Academies Press.

Paulot, F., D. Wunch, J. D. Crounse, G. Toon, D. B. Millet, P. F. DeCarlo, C. Vigouroux, N. M. Deutscher, G. González Abad, J. Notholt, et al. (2011). Importance of secondary sources in the atmospheric budgets of formic and acetic acids.

Pope III, C. A., R. T. Burnett, G. D. Thurston, M. J. Thun, E. E. Calle, D. Krewski, and J. J. Godleski (2004). Cardiovascular mortality and long-term exposure to particulate air pollution: epidemiological evidence of general pathophysiological pathways of disease. *Circulation 109*(1), 71–77.

Pye, H. O., A. Nenes, B. Alexander, A. P. Ault, M. C. Barth, S. L. Clegg, J. L. Collett Jr, K. M. Fahey, C. J. Hennigan, H. Herrmann, et al. (2019). The acidity of atmospheric particles and clouds. *UMBC Faculty Collection*.

Riemer, N., A. Ault, M. West, R. Craig, and J. Curtis (2019). Aerosol mixing state: Measurements, modeling, and impacts. *Reviews of Geophysics 57*(2), 187–249.

Sanhueza, E. and M. O. Andreae (1991). Emission of formic and acetic acids from tropical savanna soils. *Geophysical Research Letters 18*(9), 1707–1710.

Sorooshian, A., M.-L. Lu, F. J. Brechtel, H. Jonsson, G. Feingold, R. C. Flagan, and J. H. Seinfeld (2007, July). On the Source of Organic Acid Aerosol Layers above Clouds. *Environmental Science & Technology 41*(13), 4647–4654.

Sorooshian, A., N. L. Ng, A. W. H. Chan, G. Feingold, R. C. Flagan, and J. H. Seinfeld (2007, July). Particulate organic acids and overall water-soluble aerosol composition measurements from the 2006 Gulf of Mexico Atmospheric Composition and Climate Study (GoMACCS): ORGANIC ACID AEROSOL DURING GOMACCS 2006. *Journal of Geophysical Research: Atmospheres 112*(D13), n/a–n/a.

Stocker, T. F., D. Qin, G.-K. Plattner, M. Tignor, S. K. Allen, J. Boschung, A. Nauels, Y. Xia, V. Bex, P. M. Midgley, et al. (2013). Climate change 2013: The physical science basis. *Contribution of working group I to the fifth assessment report of the intergovernmental panel on climate change 1535*.

Tao, Y. and J. G. Murphy (2019, January). Evidence for the Importance of Semivolatile Organic Ammonium Salts in Ambient Particulate Matter. *Environmental Science & Technology 53*(1), 108–116.

Veres, P. R., J. M. Roberts, A. K. Cochran, J. B. Gilman, W. C. Kuster, J. S. Holloway, M. Graus, J. Flynn, B. Lefer, C. Warneke, et al. (2011). Evidence of rapid production of organic acids in an urban air mass. *Geophysical Research Letters 38*(17).

Williams, B. J., A. H. Goldstein, N. M. Kreisberg, and S. V. Hering (2010, April). In situ measurements of gas/particle-phase transitions for atmospheric semivolatile organic compounds. *Proceedings of the National Academy of Sciences 107*(15), 6676–6681.

Xu, J., J. Chen, Y. Shi, N. Zhao, X. Qin, G. Yu, J. Liu, Y. Lin, Q. Fu, R. J. Weber, et al. (2019). First continuous measurement of gaseous and particulate formic acid in a suburban area of east china: Seasonality and gas-particle partitioning. *ACS Earth and Space Chemistry*.

Yatavelli, R. L. N., H. Stark, S. L. Thompson, J. R. Kimmel, M. J. Cubison, D. A. Day, P. Campuzano-Jost, B. B. Palm, A. Hodzic, J. A. Thornton, J. T. Jayne, D. R. Worsnop, and J. L. Jimenez (2014, February). Semicontinuous measurements of gas–particle partitioning of organic acids in a ponderosa pine forest using a MOVI-HRToF-CIMS. *Atmospheric Chemistry and Physics 14*(3), 1527–1546.

Yu, S. (2000). Role of organic acids žformic, acetic, pyruvic and oxalic/ in the formation of cloud condensation nuclei žCCN/ : a review. pp. 33.

Zhang, X., A. Hecobian, M. Zheng, N. Frank, and R. Weber (2010). Biomass burning impact on $PM_{2.5}$ over the southeastern us during 2007: integrating chemically speciated frm filter measurements, modis fire counts and pmf analysis. *Atmos. Chem. Phys 10*(14), 6839–6853.